

Edge currents as a signature of flat bands in topological superconductors

Andreas P. Schnyder,^{1,*} Carsten Timm,^{2,†} and P. M. R. Brydon^{2,‡}

¹Max-Planck-Institut für Festkörperforschung, Heißenbergstrasse 1, D-70569 Stuttgart, Germany

²Institute of Theoretical Physics, Technische Universität Dresden, D-01062 Dresden, Germany

(Dated: July 31, 2021)

We study nondegenerate flat bands at the surfaces of noncentrosymmetric topological superconductors by exact diagonalization of Bogoliubov-de Gennes Hamiltonians. We show that these states are strongly spin polarized, and acquire a chiral dispersion when placed in contact with a ferromagnetic insulator. This chiral mode carries a large edge current which displays a singular dependence on the exchange-field strength. The contribution of other edge states to the current is comparably weak. We hence propose that the observation of the edge current can serve as a test of the presence of nondegenerate flat bands.

PACS numbers: 74.50.+r, 74.20.Rp, 74.25.F-, 03.65.vf

Introduction.—The bulk gap of topological insulators and superconductors plays an essential role in defining the topological invariants, and hence for the topological protection of their surface states [1–4]. Recently, however, the topological classification of matter has been extended to *gapless* systems, such as Dirac or Weyl semimetals [5, 6] and nodal superconductors [7–10]. A bulk-boundary correspondence exists for certain surfaces, yielding topologically protected dispersionless zero-energy states, so-called “arc lines” or “flat bands”. Well-known examples are the zero-energy edge states of cuprate superconductors and the A phase of ³He.

A promising materials class for topological systems is the noncentrosymmetric superconductors (NCSs), characterized by strong antisymmetric spin-orbit coupling (SOC) and a mixing of spin-singlet and spin-triplet pairing [11]. The superconducting gap in many of these compounds is reported to display line nodes, e.g., in CePt₃Si [12, 13], CeIrSi₃ [14], and Li₂(Pd_{1-x}Pt_x)₃B [15–17], and they can therefore support topological flat-band surface states. Due to the exotic gap structure of NCSs, these flat bands are predicted to be *nondegenerate*, i.e., Majorana fermions [7, 18–22], in contrast to the doubly degenerate flat bands found in other systems. Demonstrating that the surface flat bands of an NCS are nondegenerate presents a challenge, however: While typical experimental methods, such as tunneling conductance spectroscopy, are sensitive to the singular surface density of states contributed by the flat bands, they cannot probe the degeneracy.

In this Letter, we propose the response of the nondegenerate flat bands to a proximity-induced exchange field as an unambiguous test of their existence. We lay the foundation for our approach by demonstrating that the flat-band states are strongly spin polarized, which in itself is an important experimental signature. The spin polarization originates from both the SOC and the spin structure of the superconducting gap. Consistent with the time-reversal invariance of the pairing state, the spin polarization is odd in the surface momentum. Upon bringing the superconductor into contact with a ferromagnetic insulator, the flat-band states therefore acquire a *chiral* dispersion due to the coupling to the exchange field, and hence carry a sizable charge current along the interface. The current displays a remarkable singular dependence on

the exchange-field strength: Only an infinitesimal exchange field is required to generate a large current, and small changes in the external field can switch the current’s sign. In contrast, doubly degenerate flat bands, when present, give a much weaker contribution to the current. We further show that the interface current for a *fully gapped* NCS is small and not simply related to the presence of spin-polarized edge states.

Model Hamiltonian.—Quasiparticle motion in an NCS is described by the Bogoliubov-de Gennes Hamiltonian $H = \sum_{\mathbf{k}} \Psi_{\mathbf{k}}^\dagger H_{\mathbf{k}} \Psi_{\mathbf{k}}$, with $\Psi_{\mathbf{k}} = (c_{\mathbf{k}\uparrow}, c_{\mathbf{k}\downarrow}, c_{-\mathbf{k}\uparrow}^\dagger, c_{-\mathbf{k}\downarrow}^\dagger)^T$ and

$$H_{\mathbf{k}} = \begin{pmatrix} \varepsilon_{\mathbf{k}}\sigma_0 - \lambda \mathbf{l}_{\mathbf{k}} \cdot \boldsymbol{\sigma} & (\psi_{\mathbf{k}}\sigma_0 + \mathbf{d}_{\mathbf{k}} \cdot \boldsymbol{\sigma})i\sigma_y \\ -i\sigma_y(\psi_{\mathbf{k}}^*\sigma_0 + \mathbf{d}_{\mathbf{k}}^* \cdot \boldsymbol{\sigma}) & -\varepsilon_{\mathbf{k}}\sigma_0 - \lambda \mathbf{l}_{\mathbf{k}} \cdot \boldsymbol{\sigma}^* \end{pmatrix}. \quad (1)$$

Here, $\boldsymbol{\sigma}$ is the vector of Pauli matrices. The normal part of the Hamiltonian describes a two-dimensional square lattice with nearest-neighbor hopping and chemical potential μ , $\varepsilon_{\mathbf{k}} = 2t(\cos k_x + \cos k_y) - \mu$, and Rashba SOC with $\mathbf{l}_{\mathbf{k}} = \hat{\mathbf{x}} \sin k_y - \hat{\mathbf{y}} \sin k_x$ and strength λ . The even-parity spin-singlet and odd-parity spin-triplet superconducting gaps are written as $\psi_{\mathbf{k}} = \Delta_0 f(\mathbf{k}) q$ and $\mathbf{d}_{\mathbf{k}} = \Delta_0 f(\mathbf{k}) \mathbf{l}_{\mathbf{k}} (1 - q)$, respectively, where the parameter q tunes between purely spin-triplet ($q = 0$) and purely spin-singlet ($q = 1$) pairing. The structure factor $f(\mathbf{k})$ fixes the orbital-angular-momentum pairing state. Here we focus on the nodal ($d_{xy}+p$)-wave state [18] described by $f(\mathbf{k}) = \sin k_x \sin k_y$. We also present contrasting results for the fully gapped ($s+p$)-wave state [23–25] with $f(\mathbf{k}) = 1$. In our calculations we fix $(t, \mu, \lambda, \Delta_0) = (2.0, 4.0, -2.0, 0.5)$. Different values of these parameters do not qualitatively change our results.

Edge states.—The topological properties of the NCS are best revealed by examining the subgap edge states. To that end, we compute the spin- and momentum-resolved local density of states (LDOS) of Hamiltonian (1) in a ribbon of width L_x with edges perpendicular to the (10) direction. The momentum-resolved LDOS and spin-LDOS in the n -th layer are given by

$$\rho_n(E, k_y) = -\frac{1}{4\pi} \text{Im} [\text{Tr} \{G_{k_y}(n, n; E)\}], \quad (2a)$$

$$\rho_n^\mu(E, k_y) = -\frac{\hbar}{4\pi} \text{Im} [\text{Tr} \{\tilde{S}^\mu G_{k_y}(n, n; E)\}], \quad (2b)$$

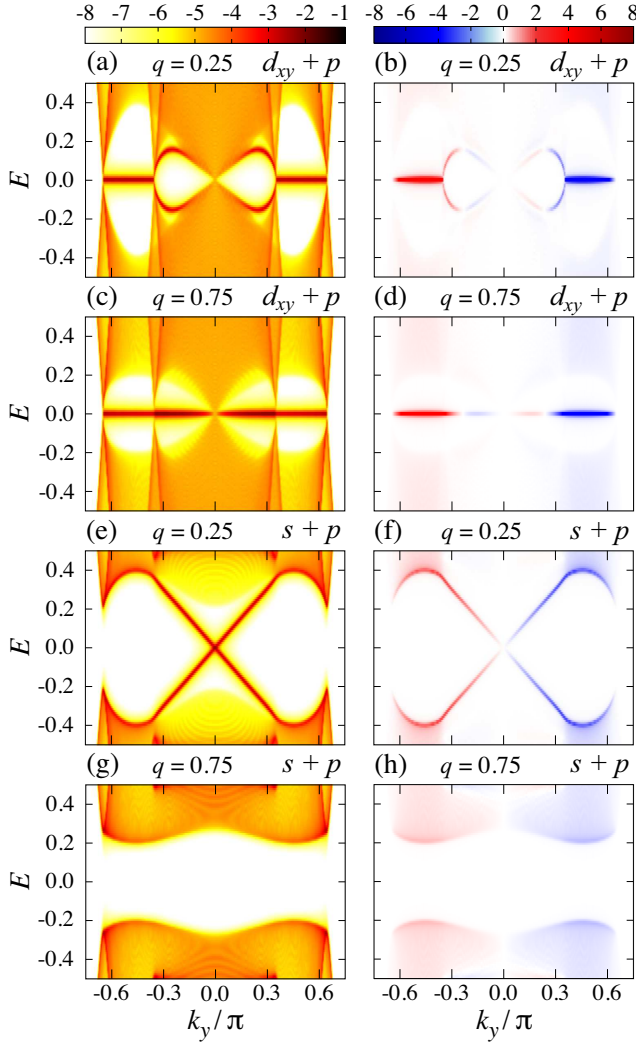


FIG. 1. (Color online) Left column: Momentum-resolved LDOS on a log scale for the ten outermost layers at the (10) edge of the $(d_{xy}+p)$ -wave NCS with (a) $q = 0.25$ and (c) $q = 0.75$, and for the $(s+p)$ -wave NCS with (e) $q = 0.25$ and (g) $q = 0.75$. In the right column we present the corresponding x component of the momentum-resolved spin-LDOS for the outermost layer in units of $\hbar/20$ on a linear scale. The z component of the momentum-resolved spin-LDOS is provided in Fig. S1 of the SM [29].

respectively, where $\tilde{S}^\mu = \text{diag}(\sigma^\mu, -[\sigma^\mu]^*)$, and $G_{k_y}(n, n'; E) = -i \int_{-\infty}^{\infty} dt e^{iEt} \langle T_t \Psi_{nk_y}(t) \Psi_{n'k_y}^\dagger(0) \rangle$ is the zero-temperature Green's function with $\Psi_{nk_y} = (2\pi L_x)^{-1/2} \sum_{\mathbf{k}_x} \Psi_{\mathbf{k}} e^{-ik_x n}$. The expressions in Eqs. (2) are evaluated for ribbons of width up to $L_x = 10^3$ and an intrinsic broadening $\eta = 0.005$. Figure 1 shows the LDOS integrated over the ten outermost layers, which is on the order of the localization length of the subgap state. Both subgap edge states (dark red/gray) and continuum bulk states (orange and yellow/light gray) are visible.

The nodal character of the $(d_{xy}+p)$ -wave state precludes the existence of a global topological number. By treating every point in the edge Brillouin zone (BZ) as the edge of a one-

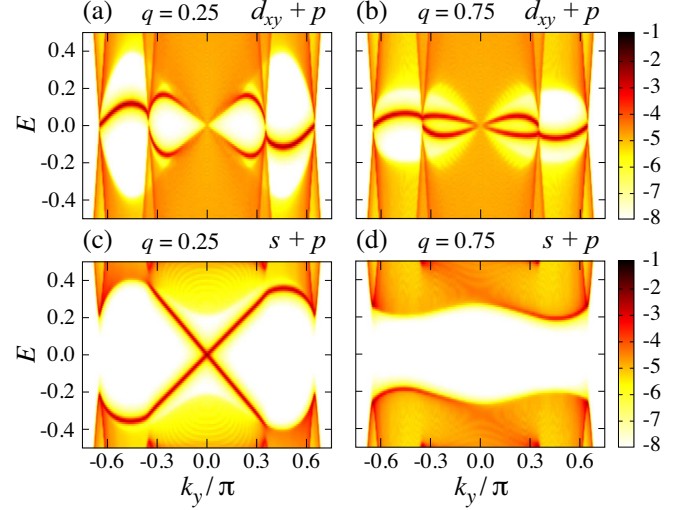


FIG. 2. (Color) Momentum-resolved LDOS at the (10) edge of (a), (b) the $(d_{xy}+p)$ -wave and (c), (d) the $(s+p)$ -wave NCS in the presence of an exchange field along the x axis with $H_{\text{ex}}^x = 0.4$, applied to the edge layer $n = 1$. In the left column we have $q = 0.25$ (majority triplet), while the right column we plot results for $q = 0.75$ (majority singlet). As in Fig. 1 we use a log color scale.

dimensional system, however, one can define a momentum-dependent winding number $W_{(10)}(k_y)$, which only changes across projected nodes of the bulk gap [7, 8, 19, 21]. In particular, one finds $W_{(10)}(k_y) = \pm 1$ for k_y lying between the projected edges $k_{F,+}$ and $k_{F,-}$ of the two spin-orbit-split Fermi surfaces, i.e., $|k_y| \in [k_{F,+}, k_{F,-}] \simeq [0.352\pi, 0.648\pi]$. This ensures the existence of nondegenerate zero-energy flat bands at these momenta k_y , which are clearly visible in Figs. 1(a) and (c). For $|k_y| < k_{F,+}$, on the other hand, there are topologically trivial dispersing states for dominant triplet pairing, and doubly degenerate zero-energy flat bands with $W_{(10)}(k_y) = \pm 2$ when singlet pairing dominates. In contrast, for $q < q_{c,L} \simeq 0.472$ and $q > q_{c,U} \simeq 0.583$, the $(s+p)$ -wave NCS is a fully gapped superconductor in symmetry class DIII. For $q < q_{c,L}$, the superconductor has a topologically nontrivial character with a non-zero \mathbb{Z}_2 topological number [2, 25, 26], and by the bulk-boundary correspondence there are helical Majorana subgap states, see Fig. 1(e) [23–25]. For $q > q_{c,U}$, the system is topologically trivial and there are no edge state [Fig. 1(g)].

Similarly to other topological systems with strong SOC [1, 27], the NCS edge states exhibit a distinct spin texture. It is well known that the electronlike part of the edge-state wavefunction is strongly spin polarized [24]. The *total* spin polarization, which includes both electronlike and holelike polarizations, is also nonvanishing. Importantly, the exchange field couples to the total spin polarization, not just to the electronlike contribution. In both NCS models we find that the continuum and subgap states show a strong total polarization in the xz spin-plane, but a vanishing y -component [28]. We present the x -spin polarization in the right-hand column

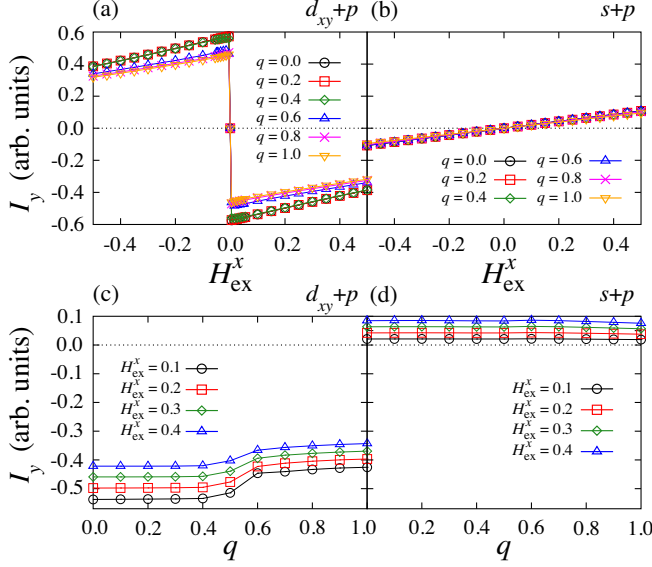


FIG. 3. (Color online) Top row: Zero-temperature edge current I_y as a function of the exchange field H_{ex}^x for various values of the singlet-triplet parameter q for (a) the $(d_{xy}+p)$ -wave and (b) the $(s+p)$ -wave NCS. Bottom row: I_y as a function of the singlet-triplet parameter q for various exchange fields along the x axis, applied to the leading edge of (c) the $(d_{xy}+p)$ -wave and (d) the $(s+p)$ -wave NCS. For comparison, the edge current of a chiral p -wave superconductor without an exchange field or SOC is about 0.64 in our units.

of Fig. 1, and the z -spin polarization in Fig. S1 of the Supplemental Material (SM) [29]. The magnitude and sign of the polarization are strongly momentum dependent, and display a complicated interplay between the singlet-triplet ratio q and the SOC strength λ . The nondegenerate zero-energy flat bands of the $(d_{xy}+p)$ -wave NCS exhibit a particularly strong and robust x -spin polarization, whereas the z -spin polarization is smaller and changes sign close to $\pm(k_{F,-} - k_{F,+})/2$ [29]. This is in contrast to the doubly degenerate states in the singlet-dominated state, which give opposite contributions to the spin-LDOS of unequal magnitude, overall leading to a weaker spin polarization than for the nondegenerate states. As required by time-reversal symmetry, subgap states with opposite edge momenta have opposite spin polarizations. This enhances the robustness of the nondegenerate flat bands, as time-reversal-invariant scattering processes connecting the oppositely x -spin-polarized states at $+k_y$ and $-k_y$ are strongly suppressed.

The nontrivial spin character of the edge states could be inferred from the absence of large- k_y backscattering processes in quasiparticle interference measurements. Another possibility is to study the response of the subgap states upon bringing the NCS into contact with a ferromagnetic insulator. We anticipate that the proximity-induced exchange field \mathbf{H}_{ex} will lead to a perturbative correction to the energy of the spin-polarized edge states proportional to $\sum_{\mu=1}^3 H_{\text{ex}}^{\mu} \rho_1^{\mu}(E, k_y)$. Since the flat-band states at $+k_y$ and $-k_y$ are oppositely spin polarized, the coupling to the exchange field will shift the en-

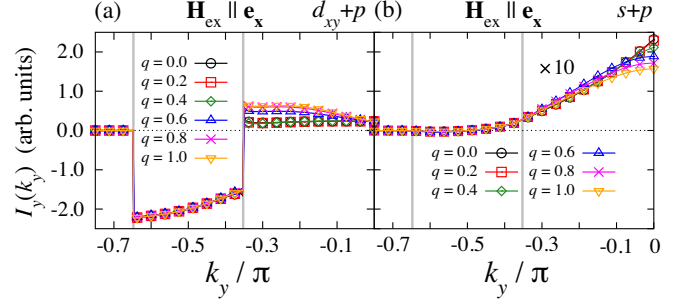


FIG. 4. (Color online) Momentum-resolved edge current $I_y(k_y)$ for various values of singlet-triplet parameter q in (a) the $(d_{xy}+p)$ -wave and (b) the $(s+p)$ -wave NCS. The exchange field is $H_{\text{ex}}^x = 0.2$. The vertical gray lines indicate the projections of the edges of the two spin-orbit-split Fermi surfaces, $|k_y| = k_{F,\pm}$. Note that the $(s+p)$ -wave results are multiplied by 10 for clarity.

ergy of these edge states in opposite directions, hence converting them into *chirally* dispersing modes. Similarly, the left- and right-moving helical edge states of the $(s+p)$ -wave NCS should acquire different velocities. To test this, we show in Fig. 2 the momentum-resolved LDOS when an exchange field $\mathbf{H}_{\text{ex}} = 0.4 \hat{x}$ is applied to the leading edge. Here and in the rest of this Letter we will specialize to an x -oriented exchange field; results for a field along the z axis are included in the SM [29]. Comparison with Fig. 1 reveals that the edge states of both NCS systems indeed display a linear shift in energy, which is to a good approximation proportional to $H_{\text{ex}}^x \rho_1^x(E, k_y)$, as long as $|H_{\text{ex}}^x| \lesssim \Delta_0$.

Edge Currents.—The chiral structure of the edge states induced by the exchange field naturally suggests the presence of a spontaneous edge current in the NCS. In particular, the chiral mode originating from the flat bands can be expected to carry a current comparable to that in a chiral p -wave superconductor. The zero-temperature expectation value of the surface component of the current is written in terms of the momentum-resolved LDOS and spin-LDOS as

$$I_y = \frac{e}{2\hbar} \frac{1}{N_y} \sum_{k_y} \sum_{n=1}^{L_x/2} \int_{-\infty}^0 dE \times \{2t \sin k_y \rho_n(E, k_y) - \lambda \cos k_y \rho_n^x(E, k_y)\}. \quad (3)$$

Here, N_y is the number of k_y points in the edge BZ. The first term in the braces is the contribution from nearest-neighbor hopping, whereas the second term is due to the SOC.

In Fig. 3 we plot the edge current I_y as a function of singlet-triplet parameter q and exchange field along the x axis. We indeed find spontaneous currents flowing along the edge of the NCS for both gap symmetries, but the two cases are dramatically different. In particular, the current in the $(d_{xy}+p)$ -wave NCS exhibits striking deviations from linear response behavior: As seen in Fig. 3(a), an infinitesimally small exchange field is sufficient to generate a large current in the NCS, and the current abruptly switches sign as the exchange field is reversed. Remarkably, the magnitude of the current

decreases with increasing exchange field from a maximum magnitude at $H_{\text{ex}}^x \rightarrow \pm 0$, which is about 90% of the one for a chiral p -wave superconductor with vanishing SOC. Although the current is somewhat larger for triplet-dominated pairing, it depends only weakly on q away from the singlet-triplet crossover ($q_{c,L} < q < q_{c,U}$), as shown in Fig. 3(c). In contrast, the current in the $(s+p)$ -wave NCS is always much smaller and grows linearly with the exchange field, see Figs. 3(b) and (d). Unexpectedly, there is almost no dependence upon the singlet-triplet parameter q , despite the qualitative change of the subgap spectrum with the topological transition at $q = q_{c,L}$.

To gain a better understanding of the origin of the currents, it is instructive to examine the current $I_y(k_y)$ contributed by states at $+k_y$ and $-k_y$, i.e., the even part of the k_y summand in Eq. (3). In Fig. 4 we show the evolution of $I_y(k_y)$ with the singlet-triplet parameter q for an exchange field along the x axis. The current in the $(d_{xy}+p)$ -wave NCS is dominated by the contribution from states with $k_{F,+} < |k_y| < k_{F,-}$, i.e., the momenta at which we find the chiral mode originating from the nondegenerate flat bands. The current displays no variation with q in this momentum range and is almost independent of the exchange-field strength (not shown), and hence accounts for most of the singular response seen in Fig. 3(a). The linear decrease of the total current with increasing exchange field originates from the contribution at $|k_y| < k_{F,+}$. Intriguingly, in this region there is also a small singular response in the singlet-dominated regime, accounting for the reduced jump in the total current in Fig. 3(a). Its origin will be discussed briefly below. The profile of $I_y(k_y)$ in the $(s+p)$ -wave NCS shows that the edge current is in this case due to states with $|k_y| < k_{F,+}$. Although this is the momentum range in which the helical edge states are realized for $q < q_{c,L}$, there is little q dependence of the momentum-resolved currents. We hence conclude that the current is largely insensitive to the helical edge states.

Discussion.—The strong edge current in the $(d_{xy}+p)$ -wave NCS is primarily carried by the chiral edge mode originating from the nondegenerate flat bands. Although the exchange field induces chiral structures in all the edge states, only this mode is *uncompensated* by a counter-propagating state. For example, even though they have different velocities, the left- and right-moving edge states in the $(s+p)$ -wave NCS still carry identical currents in opposite directions at zero temperature. This statement can be formalized by examining Eq. (3): Only the hopping term is sensitive to the chiral structure, as it is proportional to the difference between the number of states (integrated LDOS) below the Fermi energy at $+k_y$ and $-k_y$. Inspection of Fig. 2 clearly shows that only the opposite energy shift of the oppositely polarized nondegenerate flat bands can generate such a number difference. The singular behavior of the current immediately follows, as the number difference appears even for infinitesimal field strength, and does not change as the field is increased. The hopping contribution is vanishing in all other cases, and the current is instead due to the SOC term in Eq. (3), which is proportional to the sum of

the x -spin polarization at $+k_y$ and $-k_y$. This naturally connects the linear variation of the current with field strength to the induced surface magnetization.

In the case of the majority-singlet $(d_{xy}+p)$ -wave NCS, however, the splitting of the doubly degenerate flat bands for $|k_y| < k_{F,+}$ also gives a small singular response to the exchange field, as even an infinitesimal shift of the negatively (positively) spin-polarized states below (above) the Fermi energy generates a finite x -spin polarization. The current from the doubly degenerate states nevertheless increases monotonically with exchange field strength, and so the overall decreasing current remains a signature of the nondegenerate flat bands. The doubly degenerate flat bands are also distinguished by their dependence on the exchange-field orientation. While the magnitude of the current contributed by the doubly degenerate flat bands is equal for both x - and z -oriented fields, the current due to the nondegenerate flat bands undergoes a large change as the field is rotated from the x to the z axis [29].

Although we have specified our discussion to the case of an insulating ferromagnet, we note that an edge current is also induced by placing the NCS in contact with a ferromagnetic metal [30, 31]. The observation of a large edge current at the interface between an NCS and any ferromagnet would therefore be strong proof of the existence of nondegenerate flat bands. Experimental detection of the edge currents should be possible in spite of the Meissner effect, which implies that screening currents exactly compensate the edge currents in a large sample. However, whereas the edge-current density decays into the bulk on the scale of the coherence length ξ_0 , the screening only builds up over the scale of the penetration depth λ_L . For an extreme type-II superconductor, characteristic of many NCSs [11], the screening currents will therefore be suppressed in a sample of width W with $\xi_0 \ll W \ll \lambda_L$. This argument also holds for an engineered NCS [32].

Summary.—We have proposed a novel test of nondegenerate flat bands at the edge of a topological NCS based on their response to an exchange field. Specifically, we have shown that due to their strong spin polarization, they acquire a chiral dispersion when placed in contact with a ferromagnet. The resulting current shows a characteristic singular dependence upon the exchange field strength, and dominates the current due to other edge states, including doubly degenerate flat bands.

Acknowledgments.—The authors thank M. Sigrist for useful discussions. A.P.S. thanks NORDITA for its hospitality and financial support. C.T. acknowledges financial support by the Deutsche Forschungsgemeinschaft through Research Training Group GRK 1621.

* a.schnyder@fkf.mpg.de

† carsten.timm@tu-dresden.de

‡ brydon@theory.phy.tu-dresden.de

- [1] M. Hasan and C. Kane, Rev. Mod. Phys. **82**, 3045 (2010).
- [2] S. Ryu, A. P. Schnyder, A. Furusaki, and A. W. W. Ludwig, New J. Phys. **12**, 065010 (2010).
- [3] X.-L. Qi and S.-C. Zhang, Rev. Mod. Phys. **83**, 1057 (2011).
- [4] A. P. Schnyder, S. Ryu, A. Furusaki, and A. W. W. Ludwig, Phys. Rev. B **78**, 195125 (2008).
- [5] A. M. Turner and A. Vishwanath, arXiv:1301.0330.
- [6] X. Wan, A. M. Turner, A. Vishwanath and S. Y. Savrasov, Phys. Rev. B **83**, 205101 (2011).
- [7] A. P. Schnyder and S. Ryu, Phys. Rev. B **84**, 060504(R) (2011).
- [8] Y. Tanaka, M. Sato, and N. Nagaosa, J. Phys. Soc. Jpn. **81**, 011013 (2012).
- [9] Y. X. Zhao and Z. D. Wang, Phys. Rev. Lett. **110**, 240404 (2013).
- [10] S. Matsuura, P.-Y. Chang, A. P. Schnyder, and S. Ryu, New J. of Phys. **15**, 065001 (2013).
- [11] E. Bauer and M. Sigrist (eds.), *Non-Centrosymmetric Superconductors: Introduction and Overview*, Lecture Notes in Physics vol 847 (Springer, Berlin, 2012).
- [12] K. Izawa, Y. Kasahara, Y. Matsuda, K. Behnia, T. Yasuda, R. Settai, and Y. Onuki, Phys. Rev. Lett. **94**, 197002 (2005).
- [13] I. Bonalde, R. L. Robeiro, W. Brämer-Escamilla, C. Rojas, E. Bauer, A. Prokofiev, Y. Haga, T. Yasuda, and Y. Ōnuki, New J. Phys. **11**, 055054 (2009).
- [14] H. Mukuda, T. Fujii, T. Ohara, A. Harada, M. Yashima, Y. Kitaoka, Y. Okuda, R. Settai, and Y. Onuki, Phys. Rev. Lett. **100**, 107003 (2008).
- [15] H. Q. Yuan, D. F. Agterberg, N. Hayashi, P. Badica, D. Vandervelde, K. Togano, M. Sigrist, and M. B. Salamon, Phys. Rev. Lett. **97**, 017006 (2006).
- [16] M. Nishiyama, Y. Inada, and G.-Q. Zheng, Phys. Rev. Lett. **98**, 047002 (2007).
- [17] G. Eguchi, D. C. Peets, M. Kriener, S. Yonezawa, G. Bao, S. Harada, Y. Inada, G.-q. Zheng, and Y. Maeno, Phys. Rev. B **87**, 161203(R) (2013).
- [18] Y. Tanaka, Y. Mizuno, T. Yokoyama, K. Yada, and M. Sato, Phys. Rev. Lett. **105**, 097002 (2010).
- [19] M. Sato, Y. Tanaka, K. Yada, and T. Yokoyama, Phys. Rev. B **83**, 224511 (2011); K. Yada, M. Sato, Y. Tanaka, and T. Yokoyama, Phys. Rev. B **83**, 064505 (2011).
- [20] P. M. R. Brydon, A. P. Schnyder, and C. Timm, Phys. Rev. B **84**, 020501(R) (2011).
- [21] A. P. Schnyder, P. M. R. Brydon, and C. Timm, Phys. Rev. B **85**, 024522 (2012).
- [22] J. P. Dahlhaus, M. Gibertini, and C. W. J. Beenakker, Phys. Rev. B **86**, 174520 (2012).
- [23] C. Iniotakis, N. Hayashi, Y. Sawa, T. Yokoyama, U. May, Y. Tanaka, and M. Sigrist, Phys. Rev. B **76**, 012501 (2007).
- [24] A. B. Vorontsov, I. Vekhter, and M. Eschrig, Phys. Rev. Lett. **101**, 127003 (2008); Y. Tanaka, T. Yokoyama, A. V. Balatsky, and N. Nagaosa, Phys. Rev. B **79**, 060505(R) (2009); C.-K. Lu and S.-K. Yip, Phys. Rev. B **82**, 104501 (2010).
- [25] M. Sato and S. Fujimoto, Phys. Rev. B **79**, 094504 (2009).
- [26] X.-L. Qi, T. L. Hughes, S. Raghu, and S.-C. Zhang, Phys. Rev. Lett. **102**, 187001 (2009).
- [27] D. Sticlet, C. Bena, and P. Simon, Phys. Rev. Lett. **108**, 096802 (2012).
- [28] The doubly degenerate zero-energy states in both NCS models have equal and opposite y -spin polarization. Thus, although $\rho_n^y(E, k_y)$ is always vanishing, these states are split by an exchange field along the y -axis [19, 25].
- [29] See Supplemental Material for the z component of the spin-LDOS and the effect of an exchange field along the z axis.
- [30] P. M. R. Brydon, C. Timm, and A.P. Schnyder, New J. Phys. **15**, 045019 (2013).
- [31] C.-D. Ren and J. Wang, Eur. J. Phys. B **86**, 190 (2013).
- [32] S. Takei, B. M. Fregoso, V. Galitski, and S. Das Sarma, Phys. Rev. B **87**, 014504 (2013); F. Zhang, C. L. Kane, and E. J. Mele, Phys. Rev. Lett. **111**, 056402 (2013).

Supplemental Material for

“Edge currents as a signature of flat bands in topological superconductors”

Authors: Andreas P. Schnyder, Carsten Timm, and
P. M. R. Brydon

For completeness, we present in this Supplement Material the z component of the spin-LDOS at the edge of an NCS. We also study the changes in the edge band structure induced by a z -polarized exchange field in the leading edge of the NCS and determine the resulting edge currents. The results are qualitatively similar to the ones for an x -polarized exchange field, which we have discussed in the main text.

I. Edge band structure

Fig. S1 displays the z component of the energy- and momentum-resolved spin-LDOS for the outermost layer at the (10) edge of the $(d_{xy}+p)$ -wave and $(s+p)$ -wave NCS. This figure should be compared to the x component of the momentum-resolved spin-LDOS, which is depicted in Figs. 1(b), (d), (f), and (h) of the main text. As stated in the main text, both the continuum and subgap states have a strong total spin polarization in the xz spin-plane. As required by time-reversal symmetry, the total spin polarization is an odd function of edge momentum k_y . The nondegenerate zero-energy flat bands of the $(d_{xy}+p)$ -wave NCS show a particularly strong and robust x -spin polarization [Figs. 1(b) and (d)], with a weaker z -spin polarization that changes sign near $\pm(k_{F,-} - k_{F,+})/2$ [Figs. S1(a) and (b)]. The doubly degenerate states of the $(d_{xy}+p)$ -wave NCS, which appear in the region $|k_y| \in [k_{F,+}, k_{F,-}]$, give opposite contributions to the spin-LDOS of unequal magnitude. They therefore exhibit a weaker overall spin polarization than the nondegenerate states [Figs. 1(d) and S1(b)].

An exchange field applied to the leading edge of a $(d_{xy}+p)$ -wave NCS turns the nondegenerate flat bands into dispersing chiral modes. We have demonstrated this for an x -polarized exchange field in Figs. 2(a) and (b) of the main text. Figs. S2(a) and (b) show the corresponding results for an exchange field polarized along the z axis. As before, we find that the exchange field $\mathbf{H}_{\text{ex}} = 0.4 \mathbf{e}_z$ leads to an energy shift of the edge states which is proportional to $H_{\text{ex}}^z \rho_1^z(E, k_y)$. Finally, also the left- and right-moving edge states of the $(s+p)$ -wave NCS are shifted in energy due to the proximity-induced exchange field, see Fig. S2(c) and compare with Fig. 2(c) in the main text.

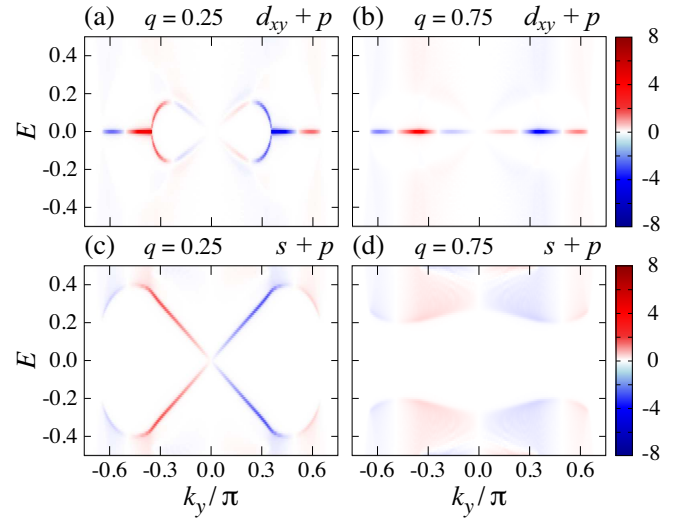


FIG. S1. z component of the energy- and momentum-resolved spin-LDOS for the outermost layer of the $(d_{xy}+p)$ -wave NCS with (a) $q = 0.25$ and (b) $q = 0.75$, and for the $(s+p)$ -wave NCS with (c) $q = 0.25$ and (d) $q = 0.75$. As in Fig. 1 of the main text the spin-LDOS is plotted in units of $\hbar/20$ on a linear scale.

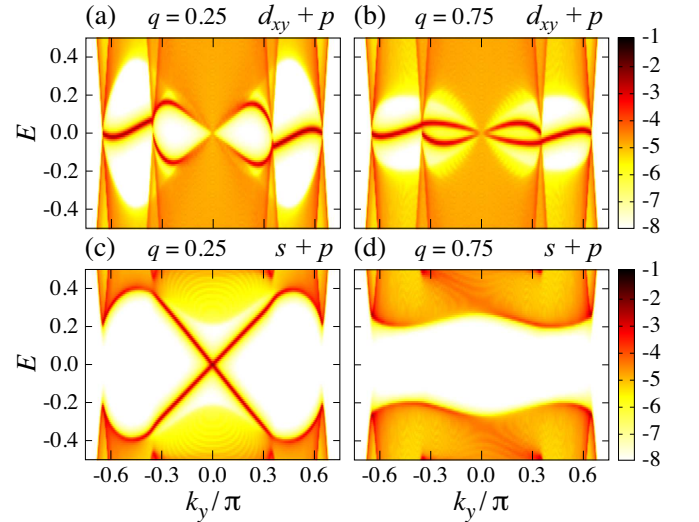


FIG. S2. Energy- and momentum-resolved LDOS on a log scale for the ten outermost layers at the (10) edge of (a), (b) the $(d_{xy}+p)$ -wave and (c), (d) the $(s+p)$ -wave NCS in the presence of a z -polarized exchange field in the leading edge with $\mathbf{H}_{\text{ex}} = 0.4 \mathbf{e}_z$. In the left column we plot the results for $q = 0.25$ (majority singlet), whereas in the right column we have $q = 0.75$ (majority triplet).

II. Edge currents

As explained in the main text, the energy shifts of the edge states induced by the exchange field lead to a spontaneous current at the edge of the NCS. We have exemplified this for an x -polarized exchange field in Fig. 3 of the main text. In Fig. S3 we present the edge current I_y for a z -polarized exchange field, as a function of singlet-triplet parameter q and exchange

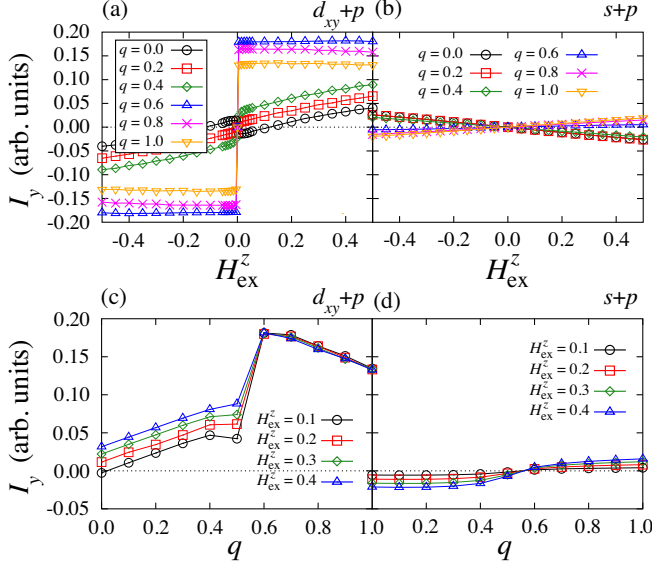


FIG. S3. Top row: Edge current I_y as a function of exchange field $\mathbf{H}_{\text{ex}} = H_{\text{ex}}^z \mathbf{e}_z$ for various values of the singlet-triplet parameter q for (a) the $(d_{xy}+p)$ -wave and (b) the $(s+p)$ -wave NCS. Bottom row: Edge current I_y as a function of singlet-triplet parameter q for various values of the exchange field $\mathbf{H}_{\text{ex}} = H_{\text{ex}}^z \mathbf{e}_z$ applied to the edge layer of (c) the $(d_{xy}+p)$ -wave and (d) the $(s+p)$ -wave NCS.

field $\mathbf{H}_{\text{ex}} = H_{\text{ex}}^z \mathbf{e}_z$. Similar to Fig. 3, we find that also a z -polarized exchange field induces a finite current both for the $(d_{xy}+p)$ -wave and the $(s+p)$ -wave NCS. As in Fig. 3(a), the current at the edge of the $(d_{xy}+p)$ -wave NCS exhibits a singular dependence on exchange-field strength [Fig. S3(a)]. The current at the edge of the $(s+p)$ -wave NCS, on the other hand, grows linearly with the exchange field, see Fig. S3(b).

Finally, in Fig. S4 we present the momentum-resolved current $I_y(k_y)$ for an exchange field polarized along the z -axis. The corresponding plot for the x -polarized exchange field is given in Fig. 4 in the main text. Interestingly, for an exchange field along the z axis the current shows a jump in $I_y(k_y)$ at the location of the sign change of the z component of the spin polarization of the nondegenerate edge states, cf. Figs. S1(a) and (b).

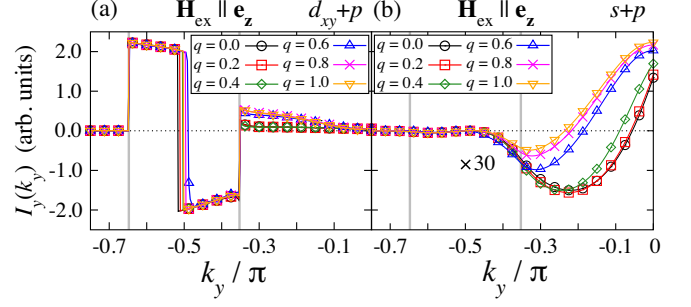


FIG. S4. Momentum-resolved edge current $I_y(k_y)$ for various values of singlet-triplet parameter q in (a) the $(d_{xy}+p)$ -wave and (b) the $(s+p)$ -wave NCS in the presence of an exchange field $\mathbf{H}_{\text{ex}} = 0.2 \mathbf{e}_z$ applied to the edge layer. The current in the $(s+p)$ -wave case has been multiplied by 30 for better visibility.